Remaining Useful Lifetime Prediction Method of Power Modules Based on the Aging Characteristic Parameters

Luhong Xie, Erping Deng, *Member, IEEE*, Dianjie Gu, Weijie Wang, Hao Liu, Ying Zhang, and Yongzhang Huang, *Member, IEEE*

***Abstract*—Remaining useful lifetime (RUL) prediction of the power module is of great significance for performing thermal management and designing effective maintenance. Since the crack is the root failure mechanism of the aging of power modules, regardless of the bond wire failure or solder layer degradation, the crack propagation process is described first and the general crack propagation law is obtained in this article. Then the general crack propagation law is extended to the general growth pattern of the aging characteristic parameters based on a simple solder layer model. After the accuracy of the general growth pattern is verified using the power cycling test results of the new and aged power module, a novel RUL prediction method is proposed based on the general growth pattern of the aging characteristic parameters. Finally, the proposed RUL prediction method is carried out on EasyPACK module, and the effectiveness of the proposed RUL prediction method is verified with the difference between the predicted lifetime and the real test lifetime lower than 2%.**

***Index Terms*—Aging characteristic parameters, power cycling test (PCT), power module, remaining useful lifetime (RUL).**

I. Introduction

SEMICONDUCTOR power modules, the main component of power electronics systems, are widely used in smart grids, new energy, rail transitions, and electric vehicles (EVs) [1]. In these applications, safety and long-term stability are the main concerns [2]. However, according to an industry survey, power electronics are the most vulnerable components, whose failure ratio to the whole system is around 31% [3]. Therefore, the reliability evaluation and remaining useful lifetime (RUL) prediction for power modules are of great significance, as they can not only prevent sudden failures but also support healthy management and operational maintenance.

The most widely used lifetime prediction method is based on the empirical lifetime model developed from a large number of power cycling lifetime data [4], [5], [6], [7], called the model-based RUL prediction method. After the lifetime model is obtained, the accumulated damage of power devices over the duration of a given mission profile can then be obtained, therewith an estimation of the expected lifetime (or RUL). Many researchers follow this method to do the lifetime prediction of power devices in different applications, such as the EVs [8], the photovoltaic inverter [9], the traction inverter [10], and the grid-side inverter [11]. However, most lifetimes are predicted based on the standard mission profile [5], or hypothetical mission profile, which means the significance of the predicted lifetime is limited due to the difference between the standard mission profile and the real operating condition. In order to obtain the real operating condition, a sensor is installed on the test rail train, and the lifetime of the IGBT power module is predicted to be 31.8 years [12]. But this lifetime is still overrated because the speed of the test rail train is lower than that of a train in service. Based on the mission profile of the electric multiple unit on the Guangzhou South-Changsha South line, the predicted lifetime of the power module in the converter is only 18.85 years [13].

Moreover, only the predicted lifetime is available, the aging process of the power module cannot be reflected. However, the aging process of the module has a great significance on the prediction results. The predicted lifetime is nearly 30.1% lower than the original value when considering the degradation of the solder layer [8].

With the development of sensor systems, data storage, and processing technology, the aging characteristic parameters that can reflect the aging of the power module in real operating conditions can be easily obtained and processed. Therefore, the data-driven lifetime prediction method has caught great concern in recent years [14], [15], [16], [17]. Based on the large amount of data extracted from the real application, an algorithm is used to study the behavior of the data acts and establish the lifetime prediction model. Neural network is currently the most popular algorithm used for lifetime prediction. The multihidden layer Elman neural network (ENN) [18], generalized regression neural network (GRNN) [19], and back propagation neural

Received 31 March 2024; revised 16 July 2024; accepted 8 September 2024. Date of publication 12 September 2024; date of current version 12 December 2024. This work was supported by the National Natural Science Foundation of China under Grant 52007061. Recommended for publication by Associate Editor Jingxin Hu. *(Corresponding author: Erping Deng.)*

Luhong Xie, Dianjie Gu, Hao Liu, Ying Zhang, and Yongzhang Huang are with the State Key Laboratory of Alternate Electrical Power System with Renewable Energy Sources, North China Electric Power University, Beijing 102206, China (e-mail: 120212101027@ncepu.edu.cn; 120222201611@ncepu.edu.cn; 120232201081@ncepu.edu.cn; 120212201137@ncepu.edu.cn; huang_y_z@ncepu.edu.cn).

Erping Deng is with the State Key Laboratory of High-Efficiency and High-Quality Conversion for Electric Power, Hefei University of Technology, Hefei 230009, China (e-mail: erping.deng@hfut.edu.cn).

Weijie Wang is with the Locomotive & Car Research Institute, China Academy of Railway Sciences Company Ltd., Beijing 100081, China (e-mail: wangweijie@zemt.cn).

Color versions of one or more figures in this article are available at https://doi.org/10.1109/TPEL.2024.3459070.

Digital Object Identifier 10.1109/TPEL.2024.3459070

network (BPNN) [20] are the commonly used algorithms to establish the lifetime prediction model. The results show that the lifetime prediction accuracy is related to the used algorithm. The prediction accuracy of the results using ENN decreased by around 0.2% compared to that using GRNN [18]. The prediction accuracy can be improved by improving the algorithm, such as the BPNN–genetic algorithms [21], the hybrid time-delay neural network [22], and the optimized long short-term memory (LSTM) networks [23]. The prediction relative accuracy of the optimized LSTM methods is up to 1.8 times that of the traditional LSTM [23]. However, the calculation process is more complicated, and more time is required to calculate [24]. Besides, due to the complexity and variability of the real operating conditions with random thermal stress, the aging characteristic parameter changes vary and are hard to predict. Therefore, a large amount of data is commonly needed, which is the biggest constraint to applying the data-driven method [17]. The accuracy of the prediction results is strongly related to the amount of used data.

Nevertheless, the lifetime prediction of power modules based on the aging characteristic parameters obtained from real operating conditions is still the most promising method, as it can effectively reflect the aging of the power module under operating conditions. According to the different aging characteristic parameters, the failure modes of the power modules can be distinguished effectively, and further optimization suggestions for the weak points of the modules can be put forward. Furthermore, regardless of the complexity of the operating conditions, the impact on the reliability of the power module is reflected in the growth of the aging characteristic parameters.

From a macro perspective, bond wire failure and solder layer degradation are the main failure modes of power modules [25]. The common symptoms of bond wire failure are foot lift-off, heel cracks, and cracks near the joint interface, whereas cracks and delamination are the main symptoms of the solder layer. Actually, the bond wire lift-off and solder layer delamination also develop from cracks regardless of packaging process defects [26], [27]. Therefore, it can be concluded that crack and its propagation are the root cause of the failure of power modules.

Aiming at the difficulty of predicting the aging characteristic parameters under complex real operating conditions, this article analyses the general law of crack propagation and extends the general law of crack propagation to the general growth law of aging characteristic parameters under constant thermal stress through a simple 2D solder layer model. Then, a conversion procedure based on the linear damage accumulation (LDA) rule is proposed to convert the aging characteristic parameters collected by the real-time electrical system with random thermal stress to that under constant thermal stress. Finally, the RUL can be predicted based on the general growth law of aging characteristic parameters. Compared with the above-mentioned RUL prediction methods, the lifetime prediction method proposed in this article has the following advantages.

1) The lifetime is predicted based on the aging characteristic parameters, which can effectively reflect the aging process of the power module.
2) According to the general growth law of aging characteristic parameters under constant thermal stress, the lifetime can be predicted easily without a large amount of data and with high precision.

The rest of the article is organized as follows. In Section II, the general law of crack propagation rate and the process of extending it to the aging characteristic parameters is described, and the general growth pattern of the aging characteristic parameters is verified using the power cycling test (PCT) results of the new and aged high power module. Section III describes the prediction procedure of the proposed RUL prediction method, which contains the conversion procedure of the aging characteristic parameters. For verifying the effectiveness and feasibility of the proposed RUL prediction method, a series of designed PCTs based on EasyPACK power modules are carried out, and the verification process is presented in Section IV. Finally, Section V concludes the article.

II. Basics of the RUL Prediction Methods

A. Crack Development

The development of cracks can be divided into two phases: 1) crack initiation phase and 2) crack propagation phase. Thus, the lifetime also consists of two parts: a crack initiation lifetime N_i, and a crack propagation lifetime N_p. In finite element analysis, the viscoplastic strain energy density growth per thermal cycle Δw_{pl} is used as the variable, Darveaux [28] defined the expression for the whole lifetime of cracks as

$$N_f = N_i + N_p = k_1 \cdot (\Delta w_{pl})^{k_2} + \frac{L_c}{da/dN} \tag{1}$$

$$\frac{da}{dN} = k_3 \cdot (\Delta w_{pl})^{k_4} \tag{2}$$

where da/dN is the propagation rate of cracks in materials, L_c is the critical length of cracks when materials fail, and k_1–k_4 are constants related to materials and structures [29].

In the field of fracture mechanics, the stress-intensity-factor range ΔK ($K_{\max}$ - $K_{\min}$) is used to describe the crack propagation rate, shown in (3) (or called Paris formula) [30], [31]

$$\frac{da}{dN} = C(\Delta K)^n \tag{3}$$

where C is a constant related to materials, and n is a numerical exponent.

According to the same expression between (2) and (3), it can be deduced that the propagation rate of cracks is constant if the applied thermal stress is fixed. This deduction is further verified by Fig. 1, which shows the crack propagation data under thermal cycling tests [28]. The slope of the curves, which means the crack propagation rate, is permanently fixed under the same test condition even though the crack has grown to a rather significant value in the later test stages. If the test conditions are changed, the crack propagation rate will change, as presented in Fig. 2, which displays the general propagation laws of the crack propagation rate. There are three stages during the crack propagation process.

1) The low-speed crack propagation stage. At this stage, there is a threshold of the stress-intensity-factor range ΔK_{th}.

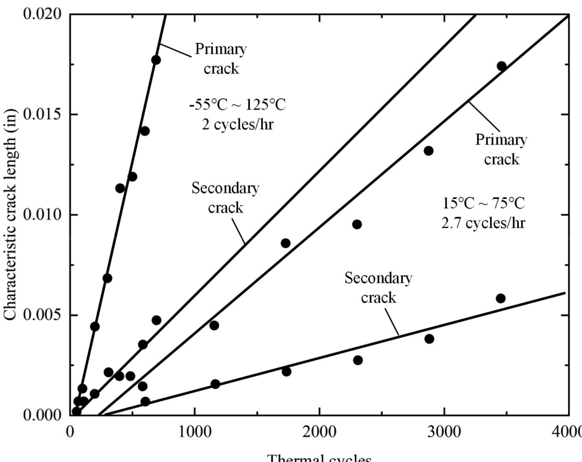

Fig. 1. Crack propagation data under thermal cycling [28].

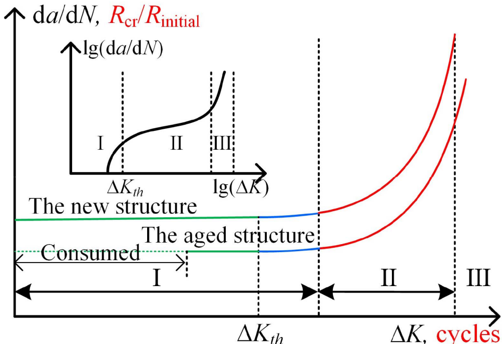

Fig. 2. Change curve of the da/dN with the changing of ΔK.

When $\Delta K \le \Delta K_{\rm th}$, the crack does not propagate, it can be considered that this stage is the initial stage of cracks. When $\Delta K > \Delta K_{\rm th}$, the crack propagates at a shallow low rate, even though it can be assumed that the crack did not propagate. Therefore, the crack propagation rate in stage I is considered as 0.

2) The stable crack propagation stage. This stage occupies most of the whole propagation process as the crack propagation at a steady rate. This stage follows the Paris formula that presents an exponential trend between da/dN and ΔK.
3) The high-speed crack propagation stage. The crack propagation rate increases sharply and enters the unstable stage, leading to the structure fracture in a short time, the lifetime of this stage, therefore, can be ignored.

According to the above analysis, the general propagation law of cracks of the new structure can be obtained, shown in Fig. 2. In stage I with low stress, the crack propagation rate is nearly zero. With the increase of stress, crack propagation enters stage II and increases exponentially.

As the crack is the root cause of the failure of power modules, the general propagation law of cracks can also be applied to power modules. However, for the power module operating in real applications, the crack propagation rate is inconsistent with the general law of crack propagation because the suffered stress is random. For the power module under PCT, since the suffered thermal stress of the power module can be obtained, the law of the crack propagation can be predicted, shown in Fig. 2, which has the same shape as the curves of the new structure but with the cycles as the x-axis.

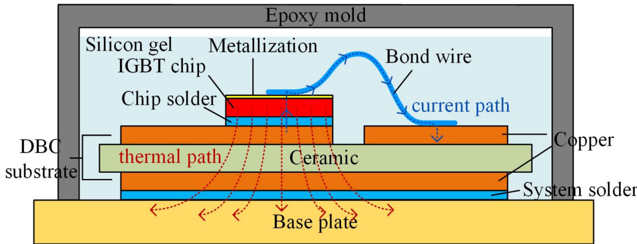

Fig. 3. Standard internal structures of power modules.

At the beginning of the test, constant test temperature conditions are set, controlled by constant power ON time $t_{\rm on}$ and power OFF time $t_{\rm off}$ [32], leading to the crack propagation rate constant. In the late test, an exponential growth of the crack propagation rate is presented due to the increased thermal stress resulting from the aging of the power module. Furthermore, for a specific power module with no manufacturing defect, the parameters in (1) and (2) are fixed, which means the initial lifetime and the exponential growth pattern are all constant, ignoring the random crack propagation. If the power module has initial cracks resulting from the manufacturing process or real operating conditions with low thermal stress, the initial lifetime will decrease, but the exponential growth pattern is not impacted, as presented in Fig. 2.

To summarize the above, two conclusions can be obtained.

1) The growth pattern of the crack propagation rate of power modules under constant thermal stress is fixed.
2) The growth pattern of the crack propagation rate of the aged power module still follows the same pattern as the new power module but with a shorter initial lifetime.

Therefore, the aging degree of the aged power module can be evaluated by comparing the crack propagation rate growth curves under the same PCT test conditions. Furthermore, the remaining lifetime of the aged power module can be predicted by processing the acquired data of the crack propagation rate since the growth pattern of the power module is fixed. However, it is impossible to predict the remaining lifetime using the crack propagation rate because cracks occur inside the structures, which are packaged by epoxy shown in Fig. 3, so they cannot be detected typically. As the aging characteristic parameters are normally used to reflect the crack of the power module, the relationship between the aging characteristic parameters and the crack propagation rate is required to be studied first.

B. Relationship Between Aging Parameters and Crack Length

Fig. 4 presents the microcracks inside the chip solder layer [33] and aluminum bond wire. Combined with the current flow path and thermal flow path of power modules shown in Fig. 3, we can see that cracks seriously impede the flow of current and

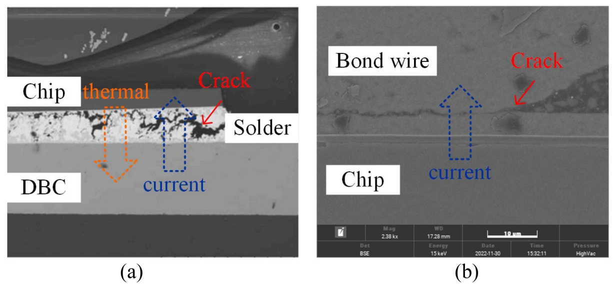

Fig. 4. SEM pictures of cracks in the chip solder layer and aluminum bond wire. (a) Chip solder layer. (b) Aluminum bond wire.

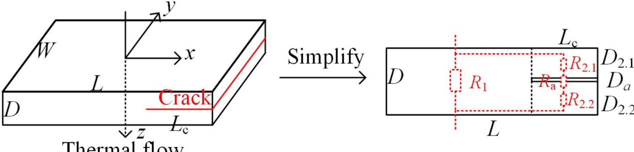

Fig. 5. Model of the solder layer with cracks.

thermal. Therefore, the electric resistance and thermal resistance can effectively reflect the crack state in the bond wire and solder layer.

Since the electric and thermal resistance have a similar calculating formula, the thermal resistance of the chip solder layer is taken as an example in this article. The analytical relationship between the thermal resistance and crack length can be obtained using mathematics. In a rectangular-shaped solder layer presented in Fig. 5, assuming that the crack propagates along the x-axis and only in the xy plane, the 3-D model can be simplified to 2-D [34]. Supposing the solder layer is complete with no internal voids or cracks, the initial thermal resistance R_{initial} of the solder can be described as

$$R_{\text{initial}} = \frac{D}{\lambda L} \tag{4}$$

where λ is the thermal conductivity of the solder alloy, D is the thickness of the solder layer, and L is the length of the solder layer.

Once the solder layer cracks, it can be considered that a layer of air is injected into the solder layer. At this time, the thermal resistance R_{cr} of the solder layer with cracks can be divided into four parts: R_1, $R_{2.1}$, $R_{2.2}$, and R_{a}, as shown in Fig. 5

$$\frac{1}{R_{cr}} = \frac{1}{R_1} + \frac{1}{R_{2.1}+R_{2.2}+R_a} = \frac{1}{R_1} + \frac{1}{R_2+R_a} = \frac{1}{\frac{D}{\lambda(L-L_c)}} + \frac{1}{\frac{D-D_a}{\lambda L_c} + \frac{D_a}{\lambda_a L_c}}. \tag{5}$$

Here, λ_a is the air thermal conductivity. L_{c} and D_{a} are the length and thickness of the crack area, respectively. Compared with the propagation of the crack length, the propagation rate of the crack thickness is small and can be considered almost constant. Moreover, the crack thickness has little effect on the thermal resistance once the crack has formed.

Since the absolute thermal resistance of the solder layer is not the interest but the change referred to the initial value, (6) is developed. As A can be considered a constant related to the solder layer geometry and materials, L_{c}/L is the only variable in (6), which represents the propagation rate of cracks da/dN. That means for power modules with a specific geometry, the thermal resistance growth rate is only affected by the crack propagation rate. Due to the growth pattern of the crack propagation rate being fixed under constant thermal stress, it can be inferred that the growth of thermal resistance is in a fixed pattern

$$\frac{R_{\text{cr}}}{R_{\text{initial}}} = \frac{L}{L-L_c+L_c\left(\frac{\lambda_a D}{\lambda_a D - D_a\lambda_a + \lambda D_a}\right)} = \frac{1}{1-\frac{L_c}{L}\left(\frac{\lambda D_a - \lambda_a D_a}{\lambda_a D - D\lambda_a + \lambda D_a}\right)} = \frac{1}{1-\frac{L_c}{L}A} = \frac{1}{1-\frac{da}{dN}A}. \tag{6}$$

In the same way, this inference can also apply to another aging characteristic parameter: electric resistance. This conclusion is the same as that manifested in the analytical model [34], that the electric resistance is only affected by the crack propagation rate as long as the geometry of the solder layer is decided, which is established based on FEA and mathematical models.

Therefore, following two inferences can be obtained.

1) The aging characteristic parameters (including thermal resistance and electric resistance) of a specific power module grow in a fixed pattern under constant thermal stress.
2) The growth of the aging characteristic parameters of the aged power module also obeys the pattern of the new one, according to the aforementioned analysis of the aged structures.

These two inferences can be described using a diagram, as shown in Fig. 2, with the growth rate $R_{\text{cr}}/R_{\text{initial}}$ of the aging characteristic parameters as the ordinate and the abscissa as the cycles. These inferences are further verified based on experimental results.

C. Experimental Verification

In order to verify the inferences, PCTs with the new power modules and the aged power modules (FZ750R65KE3) with serval service years are carried out on the test bench, shown in Fig. 10. The description of the test bench presented in Section IV-A for this verification part can be explained more briefly and clearly. Table I shows the test settings of the PCTs and the measured temperature conditions. As the temperature swing, ΔT_j is the most critical factor affecting the power cycling lifetime [35], $\Delta T_j \approx 80$ K is controlled for all of the tested power modules. To avoid random causes, six power modules are tested at the same time in each group. Group 1 is the new power module. Through comparing the curve of the aging characteristic parameters of the six modules, it can be determined whether they have a general growth pattern or not. For further verifying the growth pattern of the aging characteristic parameters, the aged

TABLE I
TEST SETTINGS OF THE POWER CYCLING TESTS

Group	Description of DUTs	t_{on}(s)	t_{off}(s)	ΔT_j (K)	T_{jmax} (°C)
1	The new power module	4	8	76.5–81.9	138.2–147.3
2	The power module with 5 years service time	4	8	75.8–81.6	122.3–132.5
3	The power module with 8 years service time	4	8	73.9–83.4	117.3–130.4

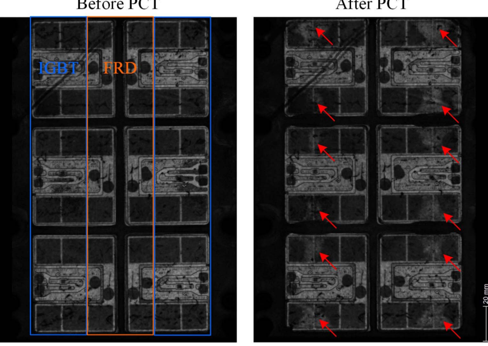

Fig. 6. SAM pictures of the chip solder layer of a new power module before and after PCT.

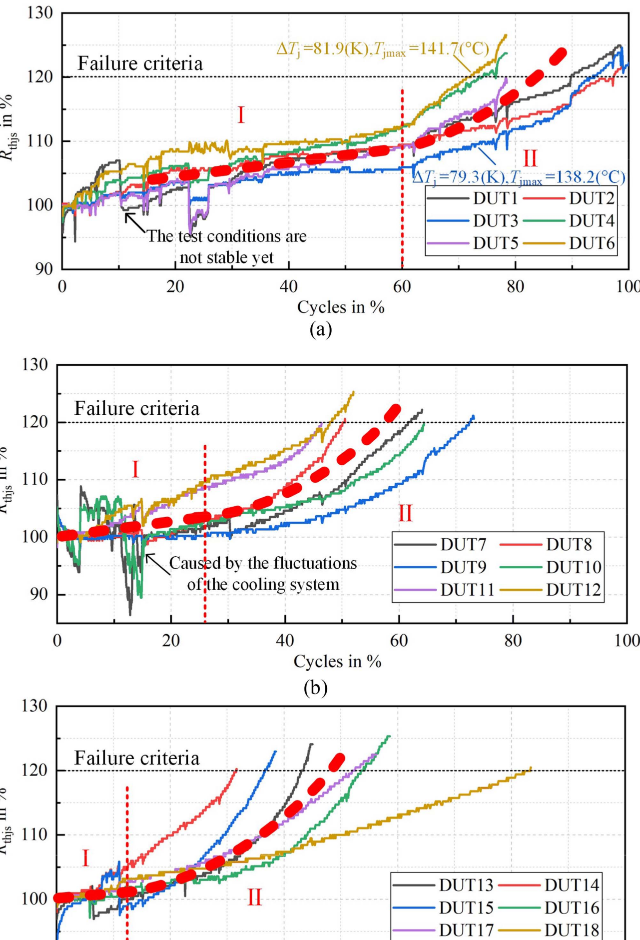

Fig. 7. Thermal resistance curves of the tested power modules. (a) New power modules. (b) Aged power modules with 5 years service time. (c) Aged power modules with 8 years service time.

power module will follow the same growth pattern as that of the new one, the aged power modules are tested in Group 2 and Group 3, which have been serviced for 5 and 8 years in real operating conditions, respectively.

During the test, the aging characteristic parameters, including the junction to heatsink thermal resistance $R_{\mathrm{th}js}$ and the power ON voltage drop V_{CE} are monitored online. As the failure criteria specified in the AQG standard [36] of that a 5% increase of V_{CE} and a 20% increase of R_{thjs} of its initial value is applied, we can obtain that the tested power modules all fail as a result of the increment of $R_{\mathrm{th}js}$, which represents the solder layer degradation with cracks. The scanning acoustic micrography (SAM) pictures further verify this conclusion, as shown in Fig. 6, with a new power module as an example. Compared with the IGBT solder layer before and after PCT, the edges of the solder layer of the IGBT chips become significantly white after PCT, meaning that cracks initiate at the edge and propagate to the center. The FRD chips are the same without aging.

The change curves of the $R_{\mathrm{th}js}$ of the tested power modules in each group are shown in Fig. 7. The cycles of each module are normalized to the power module with maximum cycles due to commercial reasons. It is clear that all six $R_{\mathrm{th}js}$ curves exhibit the same change trend depicted in Fig. 7(a), indicated by the red dotted line. Note that the increase at the beginning of the test is due to the increase in the water temperature of the cooling system because a certain time is needed for the whole test system to be stabilized. Since the maximum temperature T_{jmax} of the new power module is higher than that of the aged power module, the stabilization time is longer. However, the conclusion is not affected, and we can obtain that for a specific power module under the same thermal stress. The dispersity between the change curves of the $R_{\mathrm{th}js}$ of the six power modules is due to the different test temperature conditions. Higher test temperatures lead to faster growth rates of the $R_{\mathrm{th}js}$.

After the test conditions stabilized, the thermal resistance exhibits (I) linear low-speed growth stage, and after a specific number of cycles, it exhibits (II) polynomial high-speed growth stage. Therefore, the red dotted line can be divided into two segments. The expressions of each segment are obtained by fitting the data, which are shown in the following, respectively

$$R_{\mathrm{th}js_I} = ax + b \tag{7}$$

$$R_{\mathrm{th}js_\mathrm{II}} = cx^2 + dx + e. \tag{8}$$

Here, a, b, c, d, and e are the model parameters to be determined. x represents the power cycling cycles.

It is worth noting that the $R_{\mathrm{th}js}$ growth pattern of the new 6500 V power module is different from the normal growth pattern shown in Fig. 6 because the growth rate of the aging

characteristic parameters is affected not only by the crack propagation rate but also by the geometry parameters. That means the growth pattern of the aging characteristic parameters is different for different power modules with different geometry.

Through comparing the change curves of $R_{\mathrm{th}js}$ of the power module aged for 5 years and 8 years shown in Fig. 7(b) and (c), it can be found that the $R_{\mathrm{th}js}$ follow the same two stages as that of the new power modules. Furthermore, it is obvious that the test cycles of stage I are getting shorter with the increase in service times. This phenomenon is entirely consistent with the inference that the crack's initial lifetime of the aged power module is shorter than that of the new one, as shown in Fig. 2. Consequently, the inferences are effectively verified by experimental results.

Based on the inferences that the aging characteristic parameters of a new power module will grow in a fixed pattern under the same thermal stress, the model of the aging characteristic parameters can be established. Since the aging characteristic parameters of the aged power module will follow the same growth pattern, the aging model can be used to predict the change trend of the aging characteristic parameters by fitting the partial data, the RUL can, therefore, be predicted.

III. Description of the Conversion Process and the RUL Prediction Process

This section mainly describes the RUL prediction procedure proposed in this article. For the power module operating in real applications, the suffered thermal stress is random, leading to the aging characteristic parameters no longer growing in a fixed pattern and being hard to predict. If the growth pattern of the aging characteristic parameters is fixed, the RUL can be easily predicted. Therefore, the fixed growth pattern of the aging characteristic parameters of the power module under constant thermal stress is used in this article for RUL prediction.

The most critical step in the prediction procedure is converting the aging characteristic parameter under random thermal stress in real operating conditions to that under constant thermal stress (the target thermal stress). The LDA rule (also called Miner's rule) [37] is used in this article for the conversion.

Based on the LDA rule, the damage accumulated under real operating conditions over a time period can be considered as that suffered over a certain number of cycles under the target constant thermal stress. That means the time can be replaced by the number of cycles. At this time, the aging characteristic parameters measured during downtime or online in real applications with the time axis are converted to that with the axis of cycles. According to the growth pattern of the aging characteristic parameters with cycles under the target constant thermal stress obtained by PCT, the remaining lifetime N_{r} under the target constant thermal stress can be predicted. Then, the predicted lifetime N_{r} can be converted to the RUL under the real operating conditions by LDA.

It is worth noting that the precondition of this RUL prediction method is that the temperature profile and the aging characteristic parameters measured in real operating conditions should be obtained first. Considering this is not the focus of this

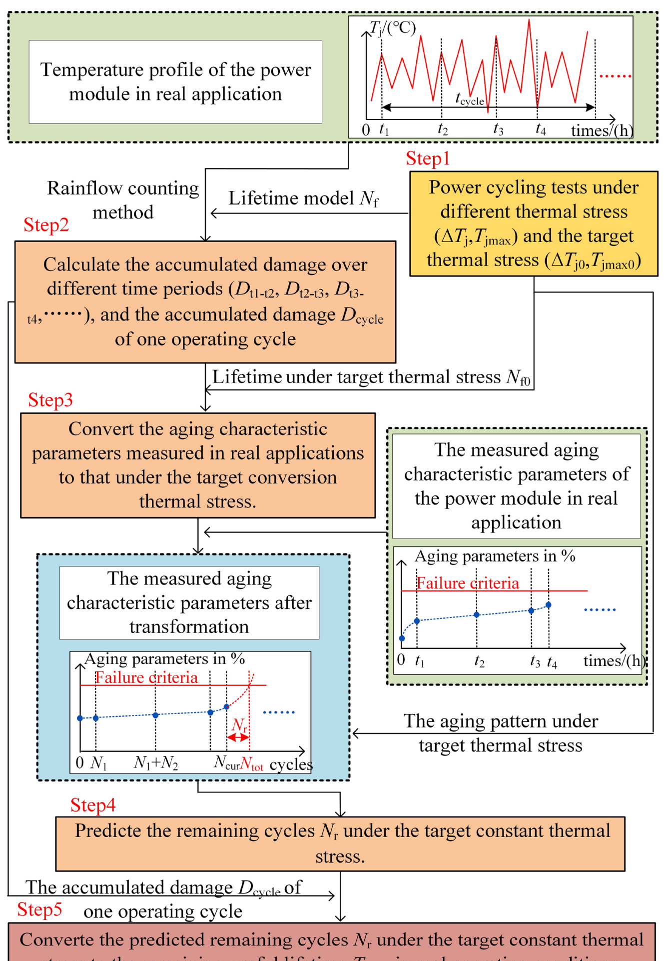

Fig. 8. RUL prediction procedure.

article but the RUL prediction method, the hypothetical data are used in this section to illustrate the prediction procedure better. However, in applying this RUL prediction method, the selection of the aging characteristic parameters will directly decide the accuracy of prediction results. This is because the sensitivity of the aging characteristic parameters to characterize different failure modes is different. For example, the collector-emitter ON-state forward voltage $V_{\mathrm{CE\text{-}on}}$ is mainly used to characterize the aging of the bond wire, while the junction-to-heatsink thermal resistance $R_{\mathrm{th}js}$ is mainly used to characterize the degradation of the solder layer. Consequently, it is vital to figure out the power module's failure mode before predicting the RUL of the power module using the proposed RUL prediction method in this article.

The RUL prediction procedure contains five steps, as shown in Fig. 8.

Step 1: A series of PCTs under different thermal stresses (ΔT_j, $T_{j\max}$) are carried out to establish the lifetime model N_f. The detailed establishing process of the lifetime model can be found in literature [35]. The lifetime N_{f0} and the growth pattern of the aging characteristic parameters under the target conversion thermal stress (ΔT_{j0}, $T_{j\max0}$) are directly obtained by PCTs.

Step 2: According to the rainflow counting method, the number $(n_1, n_2, \ldots, n_\text{p})$ of cycles under different level thermal stresses during the period from t_i to $t_{\text{i}+1}$ can be statistically obtained. Then, the accumulated damage ratio $D_{ti\text{-}ti+1}$ can be calculated as

$$D_{ti-ti+1} = \sum_{\text{p}=1}^{m} \frac{n_\text{p}}{N_{f\,p}\left(\Delta T_{jp}, T_{j\,\max p}\right)}. \tag{9}$$

Step 3: Based on the LDA rule, the accumulated damage under the random thermal stress during the period from t_i to t_{i+1} can be considered to be caused by the constant target thermal stress of a certain number of cycles N_{i+1}, shown in (10). Therefore, the aging characteristic parameters measured in real applications can be converted to that under the target conversion thermal stress. The graph of aging characteristic parameters with the number of cycles as the axis is obtained, as shown in Fig. 8.

Note that the selected target conversion thermal stress should be in the plastic zones because the thermal stress in the elastic zones will not cause damage to the power module [38]. Furthermore, considering the PCT under the target thermal stress needs to be carried out in step 1, the large target thermal stress should be selected to save the test time

$$D_{ti-ti+1} = \frac{N_{i+1}}{N_{f0}} \tag{10}$$

where $N_{\text{i}+1}$ is the number of cycles under the target thermal stress.

Step 4: Predicting the remaining cycles N_r under the target constant thermal stress. Based on the growth pattern of the aging characteristic parameters under the target thermal stress obtained by PCT, a general aging model is established in step 1 for power modules. Due to individual differences, a specific aging model should be established by fitting the converted data. Then, the total power cycling lifetime N_tot can be predicted by introducing the failure criteria to the specific aging model. Then, the remaining power cycling lifetime N_r can be obtained by subtracting the current number of cycles N_cur from the predicted total power cycling lifetime.

Step 5: Converting the predicted remaining cycles N_r under the target constant thermal stress to that under the random thermal stress in real application. Based on the LDA rule, the whole damage that the power module can withstand can be obtained by N_r/N_{f0}. Since the accumulated damage of one operating cycle D_cycle has been calculated in step 2, the number n of operating cycles that the power module can withstand can be calculated by (11). Finally, the remaining power cycling lifetime N_r is converted to the real remaining useful time T_RUL according to (12)

$$n \cdot D_\text{cycle} = \frac{N_r}{N_{f0}} \tag{11}$$

$$T_\text{RUL} = n \cdot t_\text{cycle} \tag{12}$$

where t_cycle is the time of an operating cycle.

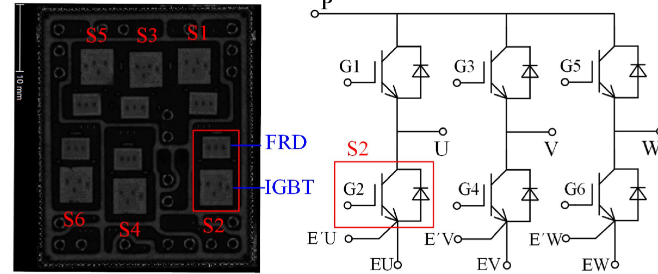

Fig. 9. EasyPACK power module under the test.

IV. Experimental Verification of the RUL Prediction Method

In this section, the proposed RUL prediction method is verified under PCTs because the lifetime of the power module under real operating conditions cannot be obtained, although the lifetime is predicted. Therefore, PCTs with varying test conditions are used to simulate the operating conditions. Then, following the prediction procedures described in Section III, the lifetime of the power module under operation conditions can be predicted. Compared with the prediction results and the experimental results, the effectiveness of the proposed RUL prediction method is verified.

Considering the long testing time for high-power modules with high reliability, normally more than 3 months for only one test condition, the EasyPACK power module (FS25R12W1T4) from Infineon is selected as the device under the test (DUT), shown in Fig. 9. The rated voltage of the EasyPACK module is 1200 V and the rated current is 25 A in the ambient temperature of 100 °C. For EasyPACK modules, six switches are packaged to form the full bridge, but only the IGBT chip of switch 2 (S2) is tested in this article.

A. PCT Strategy

Fig. 10(a) shows the test bench, which mainly contains a direct current (dc) load power supply, water cooling system, control unit, gate driver, etc. The test circuit is shown in Fig. 10(b). As we can see, there are three parallel phases. In each phase, the switches SW1, SW2, and SW3 are used to control the load current as the DUT is always ON. The control strategy is displayed in Fig. 10(c).

The control switches are switched ON successively with an overlap time of 10 μs between the adjacent phase to make sure the load current I_L flows continuously, avoiding the damage caused by drastic changes in the output to the dc power supply. Since the $V_\text{CE}(T)$ method [39] is selected to measure the junction temperature of the DUTs, a small current source is connected in parallel at the collector-emitter of the DUT to provide the measurement current I_m. Note that the measurement current I_m should be small enough to create negligible power losses, normally $I_m \approx 0.001 \cdot I_L$ is advised [40]. Therefore, the measurement current of 100 mA is used in this article. Delay time of 200 μs is set after the load current is switched OFF to measure the

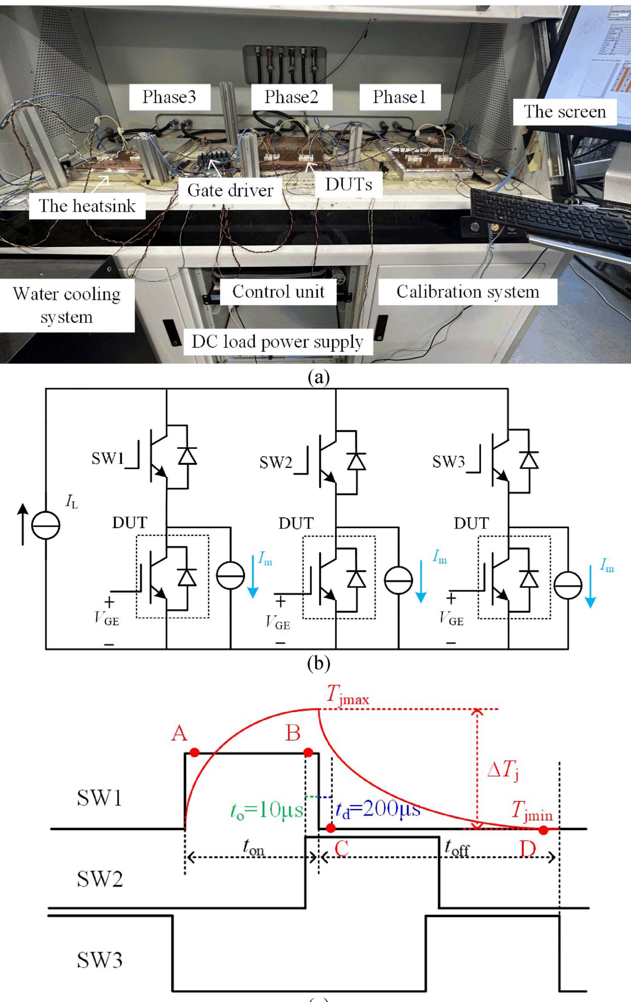

Fig. 10. Power cycling test setup. (a) Test bench. (b) Test circuit. (c) Control strategy of the test circuit.

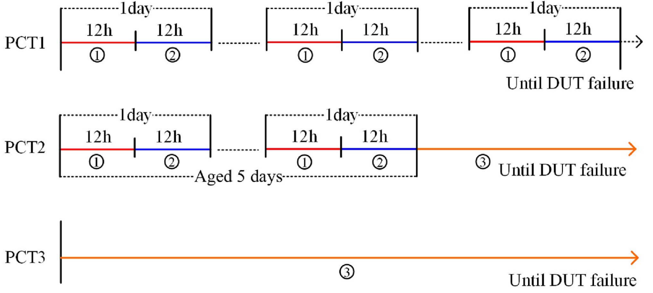

Fig. 11. Three groups of PCTs.

maximum junction temperature $T_{j\max}$ considering the inevitable carrier recombination process.

B. Test Condition Settings

Three groups of PCTs are carried out, as shown in Fig. 11. Table II presents the details of the test conditions used in PCTs. PCT 1 is used to imitate real operating conditions with random

TABLE II
TEST CONDITIONS OF PCTS

Condition	t_{on} (s)	t_{off} (s)	I_L (A)	T_s (°C)	ΔT_j (K)	T_{jmax} (°C)
1	2	4	22	62	≈ 80	≈ 150
2	2	4	20.5	62	≈ 70	≈ 140
3	2	4	23.5	62	≈ 90	≈ 150

TABLE III
ROLE OF THE PCTS

Fig.12	The connections between Fig.12 and Fig.8
PCT 1 is used to imitate real operating conditions, providing the aging characteristic parameters in real applications, which is used to be predicted.	In Fig.8: The aging characteristic parameters collected from real applications are the precondition of the RUL prediction. **However, this is hard to obtain.**
PCT 2 is used to obtain the accumulated damage ratio D_1 in a day, without using the lifetime model.	In the step 2 of Fig.8: Calculating the accumulated damage ratio $D_{ti\text{-}ti+1}$ during a period of time needs the lifetime model N_f obtained by step 1. **However, establishing the lifetime model takes a lot of time and cost.**
PCT 3 is used to obtain the lifetime N_{f3} and the growth pattern of the aging characteristic parameters under the target conversion thermal stress.	In the step 1 of Fig.8: PCT under the target thermal stress and the PCTs under different thermal stress are carried out.

thermal stress by changing temperature conditions. Considering the convenience of changing the temperature conditions, conditions 1 and 2 are used alternately to imitate the actual working conditions, each lasting for 12 h. Then one day is considered one cycle, and the aging parameters of the module are measured after each day. The water temperature T_w of conditions 1 and 2 is constant to avoid the time of the stabilization of the cooling system, leading to the temperature being changed immediately by changing the load current I_L. Condition 3 is the target conversion condition, with a higher temperature swing ΔT_j than that of conditions 1 and 2.

According to the prediction procedure described in Section III, the first step is to establish the lifetime model of the power module to calculate the accumulated damage ratio D_1 of one day. However, establishing a lifetime model requires a long time and high cost. Therefore, PCT 2 is carried out to calculate the accumulated damage ratio C_1 of one cycle based on the following according to the LDA rules

$$5 \cdot D_1 + \frac{N_3}{N_{f3}} = 1 \tag{13}$$

where N_3 is the cycle under condition 3 in PCT 2, which is obtained with $N_3 = N_{f2}$-5·$N_{1\text{day}}$. N_{f2}, and N_{f3} represent the power cycling lifetime in PCT 2 and PCT 3. $N_{1\text{day}}$ is the number of cycles of 1 day, $N_{1\text{day}} = 14400$.

PCT 3 is carried out under the target conversion temperature conditions of condition 3. So the power cycling lifetime N_{f3} and the fixed pattern of the aging characteristic parameters of the power module are obtained.

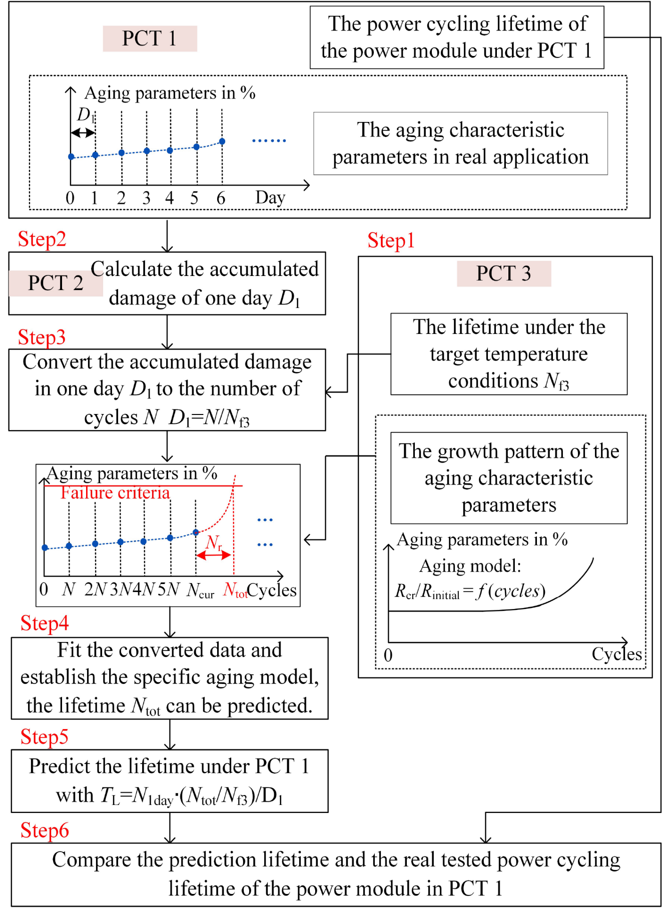

Fig. 12. Verification process.

To better understand the role of each PCT in the verification process in Fig. 12, Table III presents the function of each PCT and its connection to the steps in Fig. 8.

The steps in Figs. 8 and 12 correspond to each other, except step 6 in Fig. 12. The verification process will be carried out based on the PCT results in the next part.

C. Test Results and Verification

Table IV presents the results of three groups of PCT. Since the PCT 3 is carried out to obtain the power cycling lifetime of the power module under condition 3, six DUTs are tested at the same time to avoid the error caused by individual differences. Three DUTs are tested in PCT 1 as the sample that needs to be predicted lifetime, while three DUTs are tested in PCT 2 to obtain the mean accumulated damage in one day.

Before the verification, the failure mechanism of the test power modules should be verified as the same because the LDA is used during the verification process. Fig. 13 presents the change curves of $R_{\mathrm{th}js}$ and V_{CE} of each PCT with one DUT as an example. From Fig. 13, we can see the V_{CE} changes with the change of the test conditions because the test conditions are changed by adjusting the load current I_L. However, the $R_{\mathrm{th}js}$ are almost constant, only exponentially increasing in later stages.

TABLE IV
TEST RESULTS OF PCTS

Groups	DUTs	The measured test temperature conditions (ΔT_j, $T_{j\max}$) / (K, °C)			N_f/ cycles
		Condition 1	Condition 2	Condition 3	
PCT 1	#1	(79.2,148.3)	(70.0,139.2)	/	276 343
	#2	(78.3,146.9)	(70.3,139.1)	/	236 531
	#3	(76.4,147.4)	(68.3,139.2)	/	234 409
PCT 2	#4	(77.9,148.5)	(68.8,138.9)	(86.6,149.8)	196 267
	#5	(78.9,149.3)	(70.2,140.1)	(91.1,154.3)	198 457
	#6	(79.0,146.4)	(69.2,136.1)	(89.8,150.1)	156 823
PCT 3	#7	/	/	(89.0,148.1)	201 145
	#8	/	/	(83.6,144.4)	180 049
	#9	/	/	(91.4,152.6)	104 105
	#10	/	/	(91.1,150.4)	142 285
	#11	/	/	(88.6,152.1)	149 701
	#12	/	/	(89.7,151.8)	141 291

That is because $R_{\mathrm{th}js}$ is a calculated value by

$$R_{\mathrm{th}js} = \frac{\Delta T}{P} = \frac{T_{j\max} - T_s}{I_L \cdot V_{CE}} \approx \frac{T_{j\max} - T_{j\min}}{I_L \cdot V_{\mathrm{CE}}} = \frac{\Delta T_j}{P}. \tag{14}$$

In the case of $T_{\mathrm{S}} \approx T_{j\mathrm{min}}$, ΔT ($T_{j\mathrm{max}}$-T_S) can be considered equal to ΔT_j ($T_{j\mathrm{max}}$-$T_{j\mathrm{min}}$), while the target ΔT_j is a function of the dissipated energy which for a given chip technology is determined by the forward current and the t_{on} in the test [40]. Therefore, it can be considered that the numerator and denominator of the (13) change together, so the $R_{\mathrm{th}js}$ do not change with the change of test conditions. The exponential increment of the $R_{\mathrm{th}js}$ in the late period of PCT results from the solder layer degradation.

The SAM pictures can further verify that the degradation occurs on the chip solder layer. Compared with the solder layer before PCT, the IGBT solder layer is turned white after PCT. It is obvious that the white area representing cracks begins from the left bottom corner and propagates to the chip center. This indicates that the temperature distribution on the chip surface is not uniform. The temperature of the bottom left corner is higher than in other places, leading to the crack initiation. Since all DUTs show the same failure phenomenon, the failure mechanism can be considered the same. That means the LDA can be used here to predict the remaining lifetime.

As PCT 1 is used to simulate the real operating conditions, DUT #1 in PCT 1 is taken as an example to show the prediction process.

Step 1: PCT 3 is carried out to obtain the lifetime N_{f3} under condition 3, which is used in step 3 to calculate the accumulated damage. Therefore, a fair and accurate lifetime should be used. However, due to the difference in the test temperature conditions of the power module in PCT 3, the lifetimes show a relatively large dispersion. Therefore, it is necessary to normalize the lifetime to the same test temperature condition of $\Delta T_j = 90$ K, $T_{j\max} = 150$ °C. The lifetime of the DUTs in PCT 3 and the CIPS08 lifetime model [35], illustrated in (15), is compared, as shown in Fig. 14. It can be concluded that the lifetimes in PCT 3 follow the CIPS08 lifetime model because the round blue points represented the lifetime data of PCT 3 all around the solid line

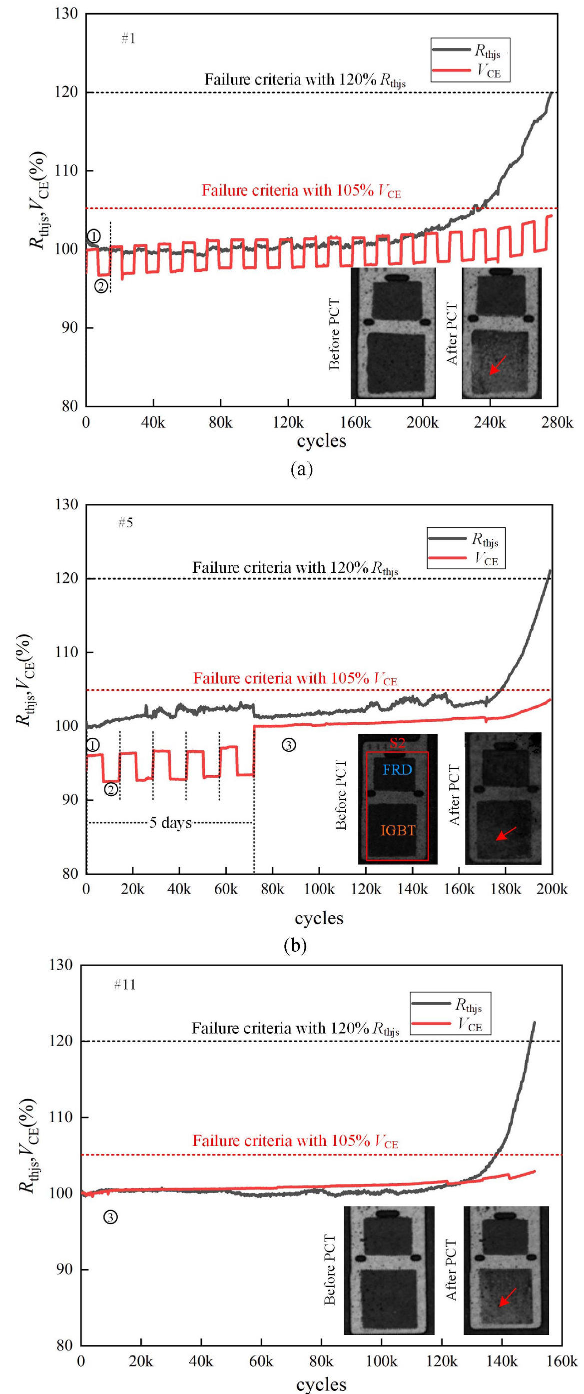

Fig. 13. Change trend of $R_{\mathrm{th}js}$ and V_{CE} during PCT. (a) DUT #1 of PCT1. (b) DUT #5 of PCT2. (c) DUT#11 of PCT3.

which represents the CIPS08 lifetime model

$$N_f = K \cdot \Delta T_j^{\beta 1} \cdot e^{\frac{\beta_2}{T_{j\min}+273}} \cdot t_{\mathrm{on}}^{\beta 3} \cdot I_b^{\beta 4} \cdot V^{\beta 5} \cdot D^{\beta 6} \quad (15)$$

where ΔT_j is the junction temperature swing, $T_{j\mathrm{min}}$ is the minimum junction temperature, t_{on} is the power ON time, I_b is the load current of each bond stitch. V is the blocking voltage of the chip, and D is the diameter of the bond wire. K and β_1-β_6 are constants fitted by experimental results [41].

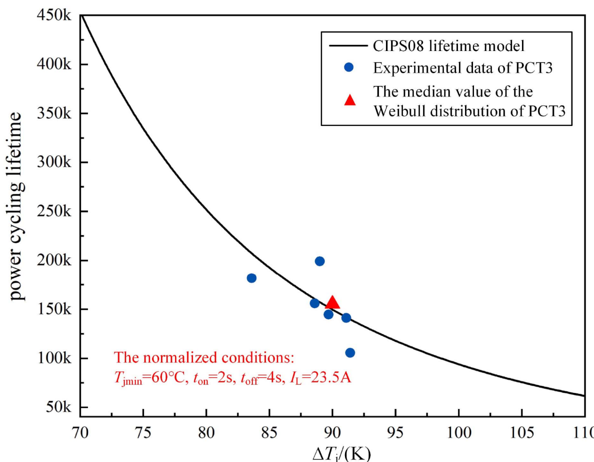

Fig. 14. Lifetime comparison between PCT 3 and CIPS08 lifetime model.

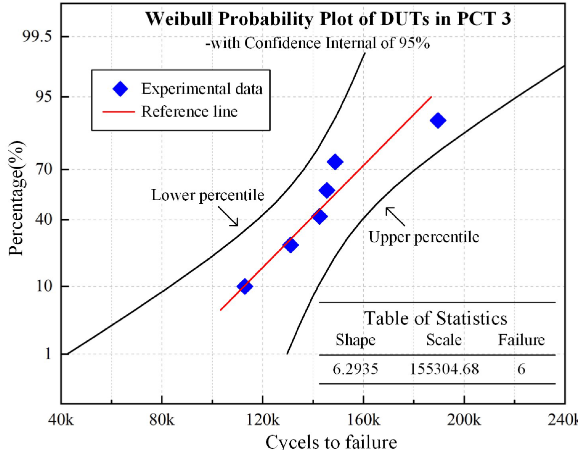

Fig. 15. Weibull distribution of the power cycling lifetime of PCT 3.

By normalizing the power cycling lifetime to the same temperature condition, the error of N_{f3} caused by different test conditions can be ignored. Furthermore, in order to avoid the error caused by individual differences, the median value of the Weibull distribution of the normalized lifetime data of PCT 3 is chosen to be the lifetime under condition 3, as shown in Fig. 15. Therefore, $N_{f3} = 155\,304$ is obtained and used in later steps.

In addition, the growth pattern of the aging characteristic parameters is obtained under condition 3, shown in Fig. 13(c). It can be obtained that the $R_{\mathrm{th}js}$ is almost constant in the early period and increases exponentially in the later period. Therefore, the aging model is established as

$$R_{\mathrm{th}js}(\%) = B + A \cdot e^{r \cdot \mathrm{cycle}}, \quad (\mathrm{cycle} > N_i) \quad (16)$$

where N_i is the number of cycles in the inflection point that separates the constant stage and exponential stage of the $R_{\mathrm{th}js}$. A, B, and r are all constants fitted by experimental data.

Note that the lifetime can be predicted only when $R_{\mathrm{th}js}$ enters the exponential growth stage, so only the aging model in the exponential growth stage is established.

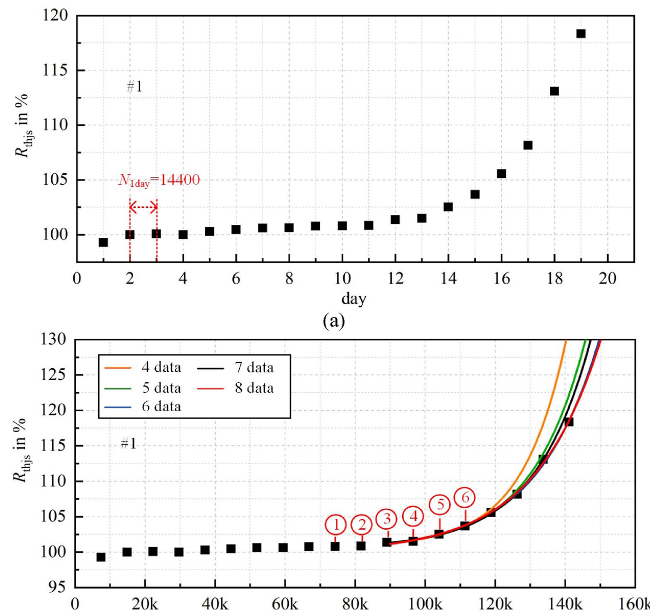

Fig. 16. $R_{\rm thjs}$ of DUT #1. (a) Before conversion. (b) After conversion.

Step 2: The accumulated damage of one day D_1 based on the results of PCT 2 is calculated. According to the LDA, the damage process of the power module can be described as

$$5 \cdot D_1 + \frac{N_{f2} - 5 \cdot N_{\rm 1day}}{N_{f3}} = 1 \tag{17}$$

where N_{f2} is the mean value of the tested cycles of PCT 2. Therefore, $D_1 = 0.04783$ is calculated.

Step 3: Convert the accumulated damage in one day D1 to the number of cycles N in the target condition 3 based on

$$D_1 = \frac{N}{N_{f3}}. \tag{18}$$

Therefore, $N = 7428$ is obtained. At this time, The $R_{{\rm th}js}$ of the DUT #1 that varies with time shown in Fig. 16(a) can be converted to that varies with the number of cycles shown in Fig. 16(b).

It should be noted that the $R_{{\rm th}js}$ of DUT #1 in PCT 1 are obtained after each cycle, as shown in Fig. 13(a). However, to make the $R_{{\rm th}js}$ curves of DUT #1 closer to the real operating conditions that $R_{{\rm th}js}$ is varied with time(day), the $R_{{\rm th}js}$ is extracted from the curves with one day (or 14 400 cycles because $N_{\rm 1day} = 14\,400$) as a period.

Step 4: Fit the converted data, the specific aging model of DUT #1 is established, therewith the lifetime $N_{\rm tot}$ can be predicted.

However, the inflection point and the numbers of data used for fitting have a great influence on the predicted lifetime. Table V presents the fitting accuracy with different inflection points shown in Fig. 16(b) and different numbers of fitting data are applied to establish the aging model. The fitting accuracy value is closer to 1, the better the fitting is. We can see from Table V that when the inflection point is fixed, the fitting accuracy is higher as more data are utilized for fitting. When the number of fitting data is fixed, the closer the inflection point is selected to the late test period, the better the fitting accuracy will be. However, since the $R_{{\rm th}js}$ develops exponentially at the late test period, the failure criterion is reached relatively soon after the inflection point. To predict the lifetime as quickly as possible, the inflection point must not be set too late, and the amount of data used for fitting should not be excessive. From Fig. 16, it can be concluded that the difference in the predicted lifetime is small when more than six data points are used.

TABLE V
FITTING ACCURACY

The inflection point	The number of the data used in fitting					
	4	5	6	7	8	9
1	/	0.9328	0.9805	0.9938	0.9970	0.9985
2	0.8676	0.9719	0.9924	0.9969	0.9983	0.9973
3	0.9503	0.9892	0.9959	0.9981	0.9969	/
4	0.9964	0.9992	0.9979	0.9971	/	/
5	0.9992	0.9986	0.9961	/	/	/
6	0.9978	0.9948	/	/	/	/

TABLE VI
PREDICTION LIFETIME

DUT	The predicted lifetime	The tested lifetime	The prediction error
#1	276 192	276 343	0.0546%
#2	239 612	236 531	1.3026%
#3	233 021	234 409	0.5921%

Consequently, point 3 is selected as the inflection point, and 6 data are used to establish the aging model as

$$R_{{\rm th}js} = 100.2145 + (6.74E - 3) \cdot e^{(5.6E-5)\cdot{\rm cycle}}. \tag{19}$$

Based on the aging model, the lifetime of DUT #1 under condition 3 is predicted with $N_{\rm tot} = 142\,460$.

Step 5: Predict the lifetime $N_{\rm L}$ under PCT 1. According to LDA, the damage caused by $N_{\rm tot} = 142\,460$ cycles under condition 3 can be converted to that under the conditions used in PCT 1 with one day as a cycle, which is described as

$$\frac{N_{\rm tot}}{N_{f3}} = n \cdot D_1. \tag{20}$$

Therefore, $n = 19.18$ days is obtained. As the cycles of one day are 14 400, we can predict the lifetime of DUT #1 under the temperature conditions used in PCT 1 is $14400 \cdot 19.18 = 276\,192$ cycles.

Step 6: Repeat the above steps, the lifetime of DUT #2 and DUT #3 in PCT 1 are predicted and displayed in Table VI.

From Table VI, we can see that the predicted lifetime based on the proposed method is almost the same as the real test lifetime with a small error lower than 2%. This conclusion can verify the effectiveness of the proposed prediction method in this article.

V. Conclusion

This article presents a novel RUL prediction method based on the general growth pattern of the aging characteristic parameters, which is extended from the general law of the crack propagation

rate based on a simple 2D solder layer model. The accuracy of the extension is verified by analyzing the PCT results of the new and aged high-power module.

Finally, a series of PCTs of the Easypack power modules are designed to carry out the proposed RUL prediction method. The effectiveness of the proposed RUL prediction method is verified by comparing the prediction lifetime and the tested lifetime.

REFERENCES

[1] H. Oh, B. Han, P. McCluskey, C. Han, and B. D. Youn, "Physics-of-failure, condition monitoring, and prognostics of insulated gate bipolar transistor modules: A review," *IEEE Trans. Power Electron.*, vol. 30, no. 5, pp. 2413–2426, May 2015.

[2] B. Lu and S. K. Sharma, "A literature review of IGBT fault diagnostic and protection methods for power inverters," *IEEE Trans. Ind. Appl.*, vol. 45, no. 5, pp. 1770–1777, Sep./Oct. 2009.

[3] S. Yang, A. Bryant, P. Mawby, D. Xiang, L. Ran, and P. Tavner, "An industry-based survey of reliability in power electronic converters," *IEEE Trans. Ind. Appl.*, vol. 47, no. 3, pp. 1441–1451, May/Jun. 2011.

[4] M. Thoben et al., "From vehicle drive cycle to reliability testing of power modules for hybrid vehicle inverter," in *Proc. PCIM Europe*, 2008, pp. 1–7.

[5] Z. Qiu, J. Zhang, P. Ning, and X. Wen, "Lifetime evaluation of inverter IGBT modules for electric vehicles mission-profile," in *Proc. 19th Int. Conf. Elect. Machines Syst.*, 2016, pp. 1–5.

[6] D. Hirschmann, D. Tissen, S. Schröder, and R. W. De Doncker, "Reliability prediction for inverters in hybrid electrical vehicles," in *Proc. 37th IEEE Power Electron. Spec. Conf.*, 2006, pp. 1–6.

[7] M. Held, P. Jacob, G. Nicoletti, P. Scacco, and M.. Poech, "Fast power cycling test of IGBT modules in traction application," in *Proc. 2nd Int. Conf. Power Electron. Drive Syst.*, 1997, vol. 1, pp. 425–430.

[8] Y. Sang, X. Wang, X. Yuan, B. Zhang, H. Wu, and J. Li, "Analysis on multiple factors influencing the lifetime of IGBTs of electric vehicles converters," in *Proc. 43rd Annu. Conf. IEEE Ind. Electron. Soc.*, 2017, pp. 882–887.

[9] P. D. Reigosa, H. Wang, Y. Yang, and F. Blaabjerg, "Prediction of bond wire fatigue of IGBTs in a PV inverter under a long-term operation," *IEEE Trans. Power Electron.*, vol. 31, no. 10, pp. 7171–7182, Oct. 2016.

[10] C. Pino et al., "Intelligent traction inverter in next generation electric vehicles: The health monitoring of silicon-carbide power modules," *IEEE Trans. Intell. Veh.*, vol. 8, no. 12, pp. 4734–4753, Dec. 2023.

[11] H. Huang and P. A. Mawby, "A lifetime estimation technique for voltage source inverters," *IEEE Trans. Power Electron.*, vol. 28, no. 8, pp. 4113–4119, Aug. 2013.

[12] W. P. Li, L. L. Zhang, W. J. Wang, and X. L. Ge, "Life evaluation of high-speed train traction rectifier IGBT module considering electric and thermal parameters update," *Railway Locomotive Car*, vol. 44, no. 2, pp. 74–78, 2022.

[13] H. Tang, W. J. Wang, Y. H. Cai, X. M. Xu, and X. L. Ge, "Life evaluation of IGBT for traction converter of high-speed train based on mission profile," *Railway Locomotive Car*, vol. 42, no. 6, pp. 89–93, 2022.

[14] C. S. Kulkarni, J. R. Celaya, G. Biswas, and K. Goebel, "Prognostics of power electronics, methods and validation experiments," in *Proc. IEEE Autotestcon*, 2012, pp. 194–199.

[15] S. Dusmez and B. Akin, "Remaining useful lifetime estimation for degraded power MOSFETs under cyclic thermal stress," in *Proc. IEEE Energy Convers. Congr. Expo.*, 2015, pp. 3846–3851.

[16] S. Dusmez, H. Duran, and B. Akin, "Remaining useful lifetime estimation for thermally stressed power MOSFETs based on on-state resistance variation," *IEEE Trans. Ind. Appl.*, vol. 52, no. 3, pp. 2554–2563, May/Jun. 2016.

[17] M. Heydarzadeh, S. Dusmez, M. Nourani, and B. Akin, "Bayesian remaining useful lifetime prediction of thermally aged power MOSFETs," in *Proc. IEEE Appl. Power Electron. Conf. Expo.*, 2017, pp. 2718–2722.

[18] Z. Y. Liu and C. L. Zhun, "IGBT life prediction based on Elman neural network model," *Semicond. Technol.*, vol. 44, no. 5, pp. 395–400, 2019.

[19] M. S. Haque, M. N. B. Shaheed, and S. Choi, "RUL estimation of power semiconductor switch using evolutionary time series prediction," in *Proc. IEEE Transp. Electrific. Conf. Expo*, 2018, pp. 564–569.

[20] M. Y. Chen et al., "Prediction of case temperature for monitoring IGBT power module using artificial neural network," *Int. Rev. Elect. Eng.*, vol. 7, pp. 3240–3247, 2012.

[21] D. Yu, "An improved prediction model of IGBT junction temperature based on back propagation neural network and Kalman Filter," *Complexity*, vol. 2021, 2021, Art. no. 5542889.

[22] A. Alghassi, S. Perinpanayagam, and M. Samie, "Stochastic RUL calculation enhanced with TDNN-based IGBT failure modeling," *IEEE Trans. Rel.*, vol. 65, no. 2, pp. 558–573, Jun. 2016.

[23] H. Ren, X. Du, Y. Yu, J. Wang, J. Zhou, and Y. Peng, "Power MOSFET lifetime prediction method based on optimized long short-term memory neural network," in *2022 IEEE Energy Convers. Congr. Expo.*, 2022, pp. 01–06.

[24] X. Yang, Y. Zhang, X. Wu, and G. Liu, "Failure mode classification of IGBT modules under power cycling tests based on data-driven machine learning framework," *IEEE Trans. Power Electron.*, vol. 38, no. 12, pp. 16130–16141, Dec. 2023.

[25] M. Junghaenel, R. Schmidt, J. Strobel, and U. Scheuermann, "Investigation on isolated failure mechanisms in active power cycle testing," in *Proc. PCIM Europe2015; Int. Exhib. Conf. Power Electron., Intell. Motion, Renewable Energy Energy Manage.*, 2015, pp. 1–8.

[26] L. H. Xie et al., "State-of-the-art of the bond wire failure mechanism and power cycling lifetime in power electronics," *Microelectronics Rel.*, vol. 147, 2023, Art. no. 115060.

[27] T. Lhommeau, C. Martin, M. Karama, R. Meuret, and M. Mermet-Guyennet, "Base-plate solder reliability study of IGBT modules for aeronautical application," in *Proc. Eur. Conf. Power Electron. Appl.*, 2007, pp. 1–10.

[28] R. Darveaux, "Effect of simulation methodology on solder joint crack growth correlation," in *Proc. 50th Electron. Compon. Technol. Conf.*, 2000, pp. 1048–1058.

[29] Z. Chen, B. Qi, J. Wang, and T. Lee, "Solution for the board level drop test in vertical direction of BGA package under ultrahigh acceleration," in *Proc. 7th Int. Conf. Electron. Packag. Technol.*, 2006, pp. 1–5.

[30] P. C. Paris and F. A. Erdogan, "Critical analysis of crack propagation laws," *J. Basic Eng.*, vol. 85, no. 4, pp. 528–533, 1963.

[31] X. Yang, J. Ye, X. Wu, K. Heng, Y. He, and G. Liu, "Lifetime prediction for lift-off of bond wires in IGBTs using Paris law with analytical calculation of crack length," *IEEE Trans. Power Electron.*, vol. 38, no. 10, pp. 13099–13110, Oct. 2023.

[32] U. Scheuermann and S. Schuler, "Power cycling results for different control strategies," *Microelectronics Rel.*, vol. 50, pp. 1203–1209, 2010.

[33] V. Smet et al., "Ageing and failure modes of IGBT modules in high-temperature power cycling," *IEEE Trans. Ind. Electron.*, vol. 58, no. 10, pp. 4931–4941, Oct. 2011.

[34] I. Gershman and J. B. Bernstein, "Solder-joint quantitative crack analysis—Ohmic resistance approach," *IEEE Trans. Compon., Packag. Manuf. Technol.*, vol. 2, no. 5, pp. 748–755, May 2012.

[35] R. Bayerer, T. Hermann, T. Licht, J. Lutz, and M. Feller, "Model for power cycling lifetime of IGBT modules—Various factors influencing lifetime," in *Proc. 5th Int. Conf. Integr. Power Electron. Syst.*, 2008, pp. 1–6.

[36] European Center for Power Electronics. Qualification of Power Modules for Use in Power Electronics Converter Units (PCUs) in Motor Vehicles. Germany: European Center for Power Electronics, AQG 324-4:2018, 2018.

[37] A. Fatemi and L. Yang, "Cumulative fatigue damage and life prediction theories: A survey of the state of the art for homogeneous materials," *Int. J. Fatigue*, vol. 20, no. 1, pp. 9–34, 1998.

[38] C. Schwabe, N. Thönelt, J. Lutz, and T. Basler, "High cycle fatigue testing of silicon IGBT devices under application-close conditions," *IEEE Trans. Power Electron.*, vol. 38, no. 11, pp. 14516–14525, Nov. 2023.

[39] R. Schmidt and U. Scheuermann, "Using the chip as a temperature sensor—The influence of steep lateral temperature gradients on the Vce(T)-measurement," in *Proc. 13th Eur. Conf. Power Electron. Appl.*, Barcelona, Spain, 2009, pp. 1–9.

[40] J. Lutz et al., *Semiconductor Power Devices*. Berlin, Germany: Springer, 2018, Art. no. 506.

[41] G. Zeng, L. Borucki, O. Wenzel, O. Schilling, and J. Lutz, "First results of development of a lifetime model for transfer molded discrete power devices," in *Proc. PCIM Europe 2018; Int. Exhib. Conf. Power Electron., Intell. Motion, Renewable Energy Energy Manage.*, 2018, pp. 1–8.

Luhong Xie was born in Jiangxi province, China, in 1996. She received the bachelor degree in electrical engineering and automation from the Hangzhou Dianzi University, Hangzhou, China, in 2018. She is currently working toward the Ph.D. degree in electrical engineering with the State Key Laboratory of Alternate Electrical Power System, Renewable Energy Sources, North China Electric Power University, Beijing, China.

Her main research interest include the failure mechanism and lifetime prediction of bond wire in power devices and reliability evaluation and the remaining lifetime prediction of the high-voltage power module.

Erping Deng (Member, IEEE) was born in Hunan province, China, in 1989. He received the bachelor degree in electrical engineering from the Harbin Institute of Technology, Harbin, China, in 2013, and the Ph.D. degree in electrical engineering from the North China Electric Power University, Beijing, China, in 2018.

He works as a Professor with Hefei University of Technology, Hefei, China, since 2022. He worked as a University Lecturer with North China Electric Power University, Beijing, China, from 2018 to 2022, and PostDoc with Chemnitz University of Technology, Chemnitz, Germany, from 2018 to 2020. His main research interest include the packaging and reliability of high voltage and high-power press pack IGBTs and now focused on the power cycling reliability, failure mechanism, lifetime modelling, and prediction of power devices.

Dianjie Gu was born in Jiangsu province, China, in 1999. He received the bachelor degree in electrical engineering from the Zhejiang University of Technology, Hangzhou, China, in 2022. He is currently working toward the master's degree in electrical engineering with the State Key Laboratory of Alternate Electrical Power System, Renewable Energy Sources, North China Electric Power University, Beijing, China.

His main research interest focuses on the packaging and reliability of power electronics.

Weijie Wang was born in Hebei province, China, in 1990. He received the B.S. degree in electrical engineering and automation and the M.E degree in electrical engineering from the Southwest Jiaotong University, Chengdu, China, in 2013 and 2015, respectively.

He is currently working as a Senior Engineer with China Academy of Railway Sciences Corporation Ltd., Beijing, China. His research interests include the power module design and the reliability of high power IGBT.

Hao Liu was born in Inner Mongolia province, China, in 2001. He received the bachelor degree in electrical engineering from the North China Electric Power University, Baoding, China, in 2023. He is currently a working toward the Ph.D. degree in electrical engineering with the State Key Laboratory of Alternate Electrical Power System, Renewable Energy Sources, North China Electric Power University.

His main research interest include the packaging and reliability of high voltage and high-power electronics devices.

Ying Zhang was born in Anhui province, China, in 1999. She received the bachelor degree in automation from the North China Electric Power University, Baoding, China, in 2021. She is currently working toward the master degree in electrical engineering with the State Key Laboratory of Alternate Electrical Power System, Renewable Energy Sources, North China Electric Power University, Beijing, China.

Her main research interest include the failure mechanism and lifetime of power devices with different material combinations.

Yongzhang Huang (Member, IEEE) received the B.S. degree in engineering physics from the Department of Engineering Physics, Tsinghua University, Beijing, China, in 1984, and the Ph.D. degree in physics from the Chinese Academy of Sciences, Beijing, China, in 1991.

He is currently a Professor with NCEPU, Beijing, China. His research interests include renewable energy power system, high-power electronic device and application, electric vehicle, and Big Data of power grid.